Product selectivity controlled by the nano-environment of Ru/ZSM-5 catalysts in nonthermal plasma catalytic CO_2 hydrogenation

Shanshan Xu [a,b,**,1], Pannida Dugkhuntod [b,c,1], Shengzhe Ding [b], Yuxin Zhang [b], Piya Gosalvitr [b], Shaowei Chen [a,d], Jianguo Huang [a], Sorasak Klinyod [c], Sarayute Chansai [b], Christopher Hardacre [b], Chularat Wattanakit [c,*], Xiaolei Fan [a,b,e,**]

[a] *Institute of Wenzhou, Zhejiang University, Wenzhou 325006, China*
[b] *Department of Chemical Engineering, School of Engineering, The University of Manchester, Oxford Road, Manchester M13 9PL, United Kingdom*
[c] *School of Energy Science and Engineering, Vidyasirimedhi Institute of Science and Technology, Rayong 21210, Thailand*
[d] *State Key Laboratory of Materials-Oriented Chemical Engineering, College of Chemical Engineering, Nanjing Tech University, Nanjing 211800, China*
[e] *Nottingham Ningbo China Beacons of Excellence Research and Innovation Institute, University of Nottingham Ningbo China, 211 Xingguang Road, Ningbo 315100, China*

ARTICLE INFO

ABSTRACT

Nonthermal plasma (NTP) systems combined with the supported metal catalyst is a promising method to enable CO_2 valorisation under mild conditions. However, insight into the relationships between the catalyst microstructure and the catalytic performance under NTP conditions is still lacking. Herein, Ru nanoparticles (NPs) on ZSM-5 zeolites with different zeolite morphologies (i.e., nanocrystals, nanosheets and conventional large crystals) and Ru NPs locations (i.e., externally supported, internally encapsulated and combination of the two) obtained by different preparation methods including encapsulation and impregnation, and combination of both approaches were investigated comparatively using NTP-catalytic CO_2 hydrogenation. The results revealed that the performance of the NTP-catalysis depends on the structure of the catalysts significantly. Specifically, ZSM-5 nanocrystal and nanosheet promoted the formation of small and highly dispersed Ru NPs (with the average particle diameters of 9–15 nm), which showed the strong interaction with CO molecule and promoted the selective CO_2 conversion to CH_4. Regarding the location of the Ru NPs, the accessibility of Ru NPs to the plasma-induced energetic species was rather important at lower input energies. Conversely, at higher input plasma energies, the intrinsic property of the Ru NPs determines the catalytic performance, and thus the 1%Ru(in) catalyst containing internally encapsulated Ru showed high CO_2 conversion of ~93% and CH_4 selectivity of ~85%, respectively. Importantly, higher input energies led to the formation of C_2H_6 via gas phase CH_4 coupling reactions.

1. Introduction

Catalytic conversion of CO_2 to value-added chemicals and fuels can be a promising method to address the issues associated with carbon emissions, benefiting the development of sustainable carbon cycling processes. CO_2 activation by thermal catalytic processes remains challenging due to the high thermodynamic stability of the linear CO_2 molecule [1]. Comparatively, nonthermal plasma (NTP) can activate stable gas molecules (such as CO_2, CH_4 and N_2) effectively in the gas

discharge to produce reactive species (i.e., ions, radicals, excited and dissociated species) which can be converted selectively over heterogeneous catalysts to target products under relatively ambient conditions. The NTP activated processes thus enable kinetically and/or thermodynamically limited chemical reactions to proceed at low pressures and temperatures [2–4]. Previously, hybrid NTP-catalysis systems have been demonstrated as an effective alternative method to conventional thermal catalysis for many reactions, such as CO_2 hydrogenation [5–7], ammonia synthesis [8,9] and water gas shift reactions [10,11].

As in thermal catalysis, the catalyst design plays an important role in NTP-catalysis and can control both the energy efficiency and product selectivity. Zeolite-supported metal catalysts are widely used in thermal heterogeneous catalysis due to their high surface area, high thermal stability, and uniform porosity [12] and are have also been found to be beneficial for NTP-catalysis. A previous study based on Monte Carlo calculations has revealed that micro-discharges might be formed near the pores of micro/mesoporous catalysts [13], hence highly porous zeolites with high specific surface areas could promote the formation of plasma micro-discharge near surface to intensify chemical conversions [3,14]. Also, the flexible pore structure could enable different catalyst designs to probe the mechanism of NTP-catalysis [15]. Previous studies have shown that the intrinsic properties of zeolite support (e.g., porous and acidic properties) strongly affect the catalyst performance in NTP-activated CO_2 hydrogenation. For example, Chen *et al.* [16] revealed that Na-form BETA zeolite benefits CO_2 adsorption compared to H-form BETA, which promoted CO_2 activation over Na-BETA supported Ni catalysts in the NTP-catalytic CO_2 methanation. Findings from the work by Bacariza *et al.* [17] show that a smaller number of Al species in the Ni/USY catalysts (i.e., a higher Si/Al ratio) was beneficial to the activity in NTP-catalytic CO_2 hydrogenation because the hydrophobic surface could repel water (which is the product from CO_2 hydrogenation) to reduce its negative effect on the reaction.

It is worth noting that a two-dimensional fluid model has predicted that plasma generation is only possible in pores with the diameter greater than the Debye length (typically >2 μm) [18], hence plasma discharge within porous zeolites is not expected to occur. Accordingly, the diffusion of the plasma-induced species to the active sites in porous materials needs to be considered carefully in catalyst design for NTP-catalysis because the reactive species are short-lived ranging from a few nanoseconds (for electronically excited atoms/molecules) to microseconds (for radicals) [19]. Previous studies on NTP-catalytic CO_2 methanation and NH_3 synthesis have demonstrated that the accessibility of the supported metal sites to the reactive species is very important during the NTP process [8,15]. Due to the complex interactions between plasma and porous catalyst, the rational design of porous zeolite-supported metal catalysts that considers the diffusion of reactive species introduced by plasma discharges for highly effective plasma-catalytic CO_2 hydrogenation deserves to be understood for NTP-catalysis.

Herein, ZSM-5 zeolites with different morphologies including nanosheets (NS), nanocrystals (NC), and conventional large crystals (Con) were first synthesized and employed to prepare Ru nanoparticles (NPs) for NTP-catalytic CO_2 hydrogenation. The effect of the support morphology on the physicochemical properties of the Ru NPs (e.g., particle size and interaction with CO_2 and CO molecules) and their catalytic performance for CO_2 hydrogenations under NTP conditions were comparatively investigated. Secondly, Ru NPs were selectively deposited on the different locations of conventional ZSM-5 zeolite (which was achieved by using different synthesis methods including encapsulation and impregnation, and combination of both approaches), and the resulting catalysts were assessed using NTP-catalytic CO_2 hydrogenation to study the effect of Ru NPs location on the catalytic selectivity. The comprehensive catalyst characterization and in situ diffuse reflectance infrared Fourier-transform spectroscopy (DRIFTS) characterization of the NTP-catalytic systems were carried out to elucidate the understand the mechanisms of the two aspects investigated.

2. Experimental

2.1. Preparation of catalysts

2.1.1. Chemicals

Tetraethyl orthosilicate (TEOS, ≥ 99.0%, Sigma-Aldrich) was used as the silica source. Tetrapropylammonium hydroxide solution (TPAOH:

40% in H_2O, Sigma-Aldrich) and tetrabutylphosphonium hydroxide solution (TBPOH, 40% in H_2O, Sigma-Aldrich) were used as the structure directing agents (SDAs). Aluminum isopropoxide (Al(O-i-Pr)$_3$, Sigma-Aldrich) and sodium aluminate (NaAlO$_2$: ≥ 98.0%, Sigma-Aldrich) were used as the alumina sources. Sodium hydroxide (Sigma-Aldrich) and ethylenediamine (EDA: 99%, Fluorochem) were used as a mineralizer and a stabilizing agent, respectively. Ruthenium (III) chloride hydrate (99.98% trace metal basis, Sigma-Aldrich) was used as the Ru precursor for catalyst preparation. All chemicals were used as received.

2.1.2. ZSM-5 nanosheets (NS)

The ZSM-5 NS was synthesised based on a molar ratio of 60 SiO_2: 0.30 Al_2O_3: 18 TBPOH: 0.75 NaOH: 600H_2O: 240 C_2H_5OH. Tetraethyl orthosilicate (TEOS) (8.7 g) was mixed with aluminum isopropoxide (0.1 g) and tetrabutylphosphonium hydroxide (8.6 g) and stirred for 10 min at room temperature (RT). Sodium hydroxide (NaOH) (0.02 g) was dissolved by 2.3 g of deionized (DI) water and was added into the above mixture. The solution was stirred continuously for 12 h at RT and transferred to an autoclave for hydrothermal synthesis at 130 °C for 2 days. The product was obtained by centrifugation and washed until pH = 7, dried overnight at 110 °C and calcined at 550 °C for 8 h.

2.1.3. ZSM-5 nanocrystal (NC)

The ZSM-5 NC was prepared by mixing TEOS (4.3 g), tetrapropylammonium hydroxide solution (TPAOH, 4.3 g), sodium aluminate (0.02 g) and water (4.78 g) with a molar ratio of 1.0SiO_2: 0.005Al_2O_3: 0.4TPAOH: 19.5 H_2O: 4 C_2H_5OH. The mixture was stirred at RT for 24 h and then was transferred to an autoclave and crystallized at 100 °C for 24 h. The solid was separated by centrifugation at 9500 rpm then washed using DI water until the pH of filtrate was approximately 7. The collected product was dried overnight at 110 °C and calcined at 550 °C for 6 h.

2.1.4. Conventional ZSM-5 (Con) crystal

The ZSM-5 Con was synthesized using a molar ratio of 10SiO_2: 0.083Al_2O_3: 1.0TPAOH: 1.03NaOH: 400 H_2O: 40 C_2H_5OH. In detail, TEOS, TPAOH and DI water was mixed to prepare the first mixture. Sodium aluminate was added to the NaOH solution to prepare the second mixture. Then the second mixture was added to the first mixture dropwise. The final mixture was stirred for 2 h at RT. The mixed solution was transferred to the autoclave and crystallized at 180 °C for 3 days. After that, it was filtered and washed until pH = 7, dried overnight at 110 °C and calcined at 550 °C for 6 h.

2.1.5. Supported Ru catalyst on external surface of ZSM-5 zeolites

Supported Ru NPs (theoretical loading of 0.5 wt% and 1.0 wt%) on the ZSM-5 zeolites above were prepared by incipient wet impregnation. Typically, 1.0 g of the calcined support was suspended in DI water (10 mL), and the precursor solution was prepared by dissolving RuCl$_3$·3 H_2O in 10 mL DI water (the concentration of the precursor solution depended on the metal loading). The precursor solution was then added to the zeolite suspension, and the mixture was stirred vigorously for 6 h. After synthesis, the mixture was dried by an evaporator at 60 °C and at 110 °C in an oven overnight. The obtained solid was calcined in a muffle furnace at 550 °C for 4 h (1 °C min^{-1}). The resulting samples are denoted as *x*%Ru(out)/NS, *x*%Ru(out)/Con and *x*%Ru(out)/NC, respectively, where *x* refers to the theoretical Ru loading.

2.1.6. Encapsulated Ru catalyst within ZSM-5 Con

The encapsulated Ru catalysts in ZSM-5 Con (theoretical loading of 0.5 wt% and 1.0 wt%) were prepared using ethylenediamine coordinated Ru, i.e., [Ru(NH$_2$CH$_2$CH$_2$NH$_2$)$_3$](Cl$_2$)$_x$, as the precursor with the molar composition of 10SiO_2: 0.083Al_2O_3: 1.0TPAOH: 1.03NaOH: 400 H_2O: 40 C_2H_5OH: *x*Ru, (where *x* is 0.03 and 0.06, respectively, for the 0.5 wt% and 1.0 wt% Ru catalysts). The synthesis condition is similar to

the method which has been used for preparing ZSM-5 Con zeolite as described above. $[Ru(NH_2CH_2CH_2NH_2)_3](Cl_2)_x$ was prepared by dissolving 0.01 g of $RuCl_3 \cdot 3 H_2O$ into 0.2 mL ethylenediamine and 2 mL H_2O mixture under stirring at RT. Then the precursor solution was added dropwise into the Con synthesis solution under stirring for 30 min. After that, the mixture was transferred into a Teflon-lined autoclave for synthesis at 180 °C for 3 days. The prepared solid products were centrifuged, washed with DI water several times, and then dried at 110 °C in the oven overnight. Finally, the obtained sample was calcined in a muffle furnace at 550 °C for 6 h to remove the organic precursor and template. The resulting sample is denoted as x%Ru(in)/Con (where x refers to the theoretical Ru loading).

For the Ru catalyst dispersed on both sides of ZSM-5, the x%Ru(in)/Con sample (~1 g) was suspended in 10 mL $RuCl_3 \cdot 3 H_2O$ solution, then stirred vigorously for 6 h. After that, the sample was dried by an evaporator at 60 °C and then calcined at 550 °C for 4 h to get the x%Ru(in)x%Ru(out)/Con catalyst.

2.2. NTP-catalytic CO_2 hydrogenation

The catalytic activity of the prepared catalysts was assessed at atmospheric pressure in a dielectric barrier discharge reactor (DBD, 6 mm O.D. × 4 mm I.D.). The discharge length and gap of the DBD reactor were 10 mm and 1.5 mm, respectively. Typically, ~100 mg catalysts (pelletised with particle size range of 250–425 μm) were loaded in the discharge zone between two quartz wool plugs. Before the catalysis, the catalysts were reduced in situ by H_2 plasma (i.e., 80% H_2/Ar at 50 mL min^{-1}) at specific input energy of 19 J mL^{-1} for 30 min. Subsequently, gas mixture of CO_2: H_2: Ar (molar ratio = 1:4:5) was fed into the DBD plasma reactor (total flowrate = 50 mL min^{-1}) to start the reaction. The specific input energy was varied from 16 to 32 J mL^{-1} (corresponding to an applied voltage of 5.5–7.0 kV). The outlet gas composition was analysed by a two-channel on-line gas chromatography (GC, PerkinElmer, Clarus 590 model) equipped with a thermal conductivity detector (TCD) and a flame ionization detector (FID). For each measurement, three samples of gas products were taken and analysed under steady-state conditions. Control experiments, i.e., NTP alone system without a catalyst (gas phase reactions) and NTP-assisted CO_2 hydrogenation over the bare zeolite supports, were performed under the same conditions. Calculation of equilibrium CO and CH_4 product distribution as a function of reaction temperature at atmospheric pressure using Aspen Plus V12.1 (PENG-ROB property method and thermodynamic equilibrium calculation using RGibbs reactor model). The bulk temperature of the DBD reactor was measured by an infrared (IR) thermometer.

2.3. In situ DRIFTS-MS characterisation

The surface species adsorbed on the catalyst surface during the NTP-assisted CO_2 hydrogenation were studied using in situ diffuse reflectance infrared Fourier transform spectroscopy-mass spectrometry (DRIFTS-MS). In situ DRIFTS measurements were performed using a Bruker Vertex 70 FTIR spectrometer, equipped with a liquid N_2-cooled mercury–cadmium–telluride detector. Typically, 50 mg catalyst were loaded into the flow cell and pre-treated under 15%H_2/Ar at 5 kV and 27.2 kHz for 15 min. Then the gas feed (H_2/CO_2 = 4 diluted in 90% Ar) at 60 mL min^{-1} was introduced into the cell. The use of Ar balance in DRIFTS was to avoid the signal saturation of IR spectra and MS signal. The experiment was conducted at an applied voltage of 5 kV and frequency of 27.2 kHz to prevent arcing. DRIFTS spectra were recorded every 30 s and analysed by the OPUS software. During the experiment, mass spectrometer (Hiden Analytical HPR20) was employed to analyse the gases (CO_2, CO, CH_4) exiting from the DRIFTS cell.

3. Results and discussion

3.1. Effect of zeolite morphology

The performance of the 1%Ru(out)/NS, 1%Ru(out)/Con and 1%Ru(out)/NC catalysts under NTP-activated CO_2 hydrogenation conditions was studied and compared with two control experiments. The gas phase NTP reaction in the absence of the catalyst showed a low CO_2 conversion of < 13.6% and 100% selectivity to CO regardless of the specific input energy (SIE) used. Similarly, the NTP systems employing the packing of bare zeolite supports was only selective to CO; however, higher CO_2 conversions of 20.7%, 23.5%, 23.9% at 32 J mL^{-1} for NC, NS and Con, respectively, were achieved (Fig. S1, due to the enhanced plasma surface discharge [20]).

Comparatively, the NTP-catalysis systems with the supported Ru catalysts showed significantly increased CO_2 conversions and improved selectivity to CH_4 and the C_2 product (C_2H_6). Regardless of the zeolite morphology, CO_2 conversions over all the supported Ru catalysts increased with an increase in SIE, suggesting a higher specific energy input facilitated CO_2 conversion (Fig. 1a). Interestingly, it was found that the zeolite morphology had a considerable effect on the catalytic performance of the Ru catalysts under the NTP conditions. The CO_2 conversions over the supported Ru catalysts follow the order of 1%Ru(out)/NC > 1%Ru(out)/NS > 1%Ru(out)/Con, and the Ru catalysts supported on NC and NS were much more capable of converting CO_2 than that on Con ZSM-5 which achieved CO_2 conversions of < 18% (Fig. 1a). Regarding the selectivity, as shown in Fig. 1b–d, CO and CH_4 were measured as the main products from the system using the 1%Ru(out)/Con catalyst, i.e., CO selectivity of 69.9–53.3% and methane selectivity of 20–45.5% selectivity, respectively.

Conversely, the 1%Ru(out)/NC and 1%Ru(out)/NS catalysts were selective to CH_4 with C_2H_6 and CO as the other products. 1%Ru(out)/NC was the most active catalyst here to convert CO_2 under the NTP conditions, and an increase in SIE led to an improved CO_2 conversion with the highest value of 83.4% achieved at an SIE of 32 J mL^{-1}. However, the selectivity to CH_4 over 1%Ru(out)/NC decreased (from 88.8% to 74%) by increasing the SIE from 21 to 32 J mL^{-1}, Fig. 1c, which was accompanied by an increase in the selectivity to C_2H_6 from 5.6% to 14.5% at SIE of 32 J mL^{-1}, Fig. 1d. The increased production of C_2H_6 can be attributed to methane coupling reactions in the gas phase which is thought to occur at a higher input energy in the gas phase [21,22]. Similar trends in CO_2 conversion and product selectivity were found in the system using the 1%Ru(out)/NS catalyst as well, as shown in Fig. 1c. However, compared to 1%Ru(out)/NC, 1%Ru(out)/NS was less active in converting CO_2 (e.g., 42.8% vs. 83.2% at 26 J mL^{-1}) but was found to be more selective to CH_4 (e.g., 84% vs. 77.6% at 26 J mL^{-1}). Considering all the catalysts having the similar Ru loading, the measured catalytic performance suggests that the morphology of the zeolite supports played a rather significant role in controlling the substrate conversion and product selectivity in NTP-catalytic CO_2 hydrogenation.

To understand the effect of zeolite morphology on the catalytic activity of the associated catalysts, extensive characterisation was carried out to investigate the characteristics of the catalysts, which will be correlated with the activity in CO_2 hydrogenation under NTP conditions. XRD analysis (Fig. S2) showed the characteristic diffraction peaks of MFI zeolite structure at 2θ of 7.8, 8.7, 23.1, and 23.8°, corresponding to the (101), (111), (501), and (303) facets, respectively, for all the catalysts (calcined) [23]. Additionally, a small peak for the RuO_2 phase at 35 ° was observed in all the three catalysts. SEM (Fig. S3) and TEM images (Fig. 2a–c) of the ZSM-5 NC and Con support show the coffin-shaped crystals with the average crystal sizes of ~120 nm and ~621 nm, respectively, whilst the ZSM-5 NS support exhibits spherical assemblies (of ~120 nm) consisting of thin zeolitic nanolayers.

The morphology and size distribution of the supported Ru nanoparticles (NPs) of the reduced catalysts were further investigated by STEM (Fig. 2d–f). For 1%Ru(out)/NC, Ru NPs with an average particle
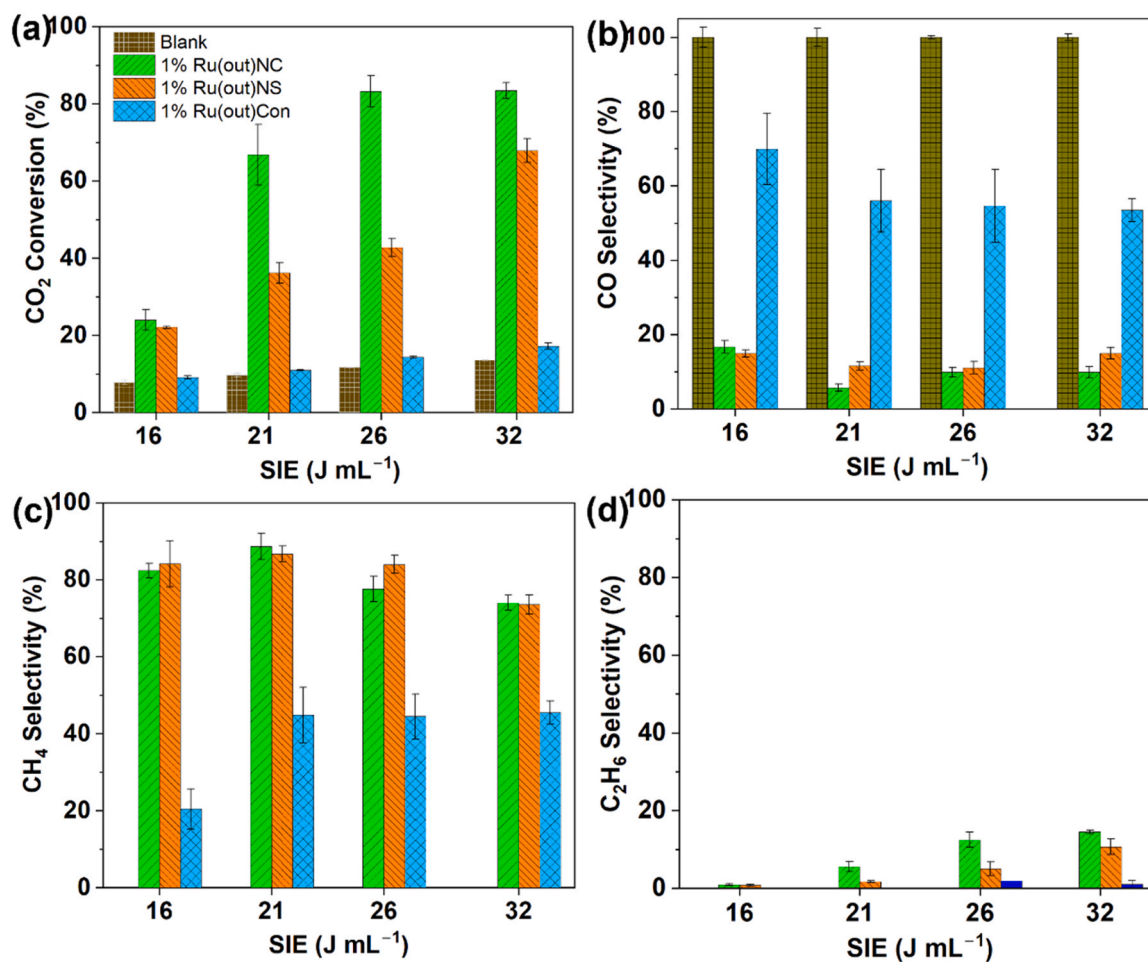
Fig. 1. Performance of NTP-activated CO_2 hydrogenation as a function of specific input energy (SIE) in NTP alone system and systems employing 1 wt% Ru supported on the ZSM-5 nanocrystal, nanosheet and conventional ZSM-5 supports (i.e., 1%Ru(out)/NC, 1%Ru(out)/NS and 1%Ru(out)/Con): (a) CO_2 conversion, (b) CO selectivity, (c) CH_4 selectivity and (d) C_2H_6 selectivity.
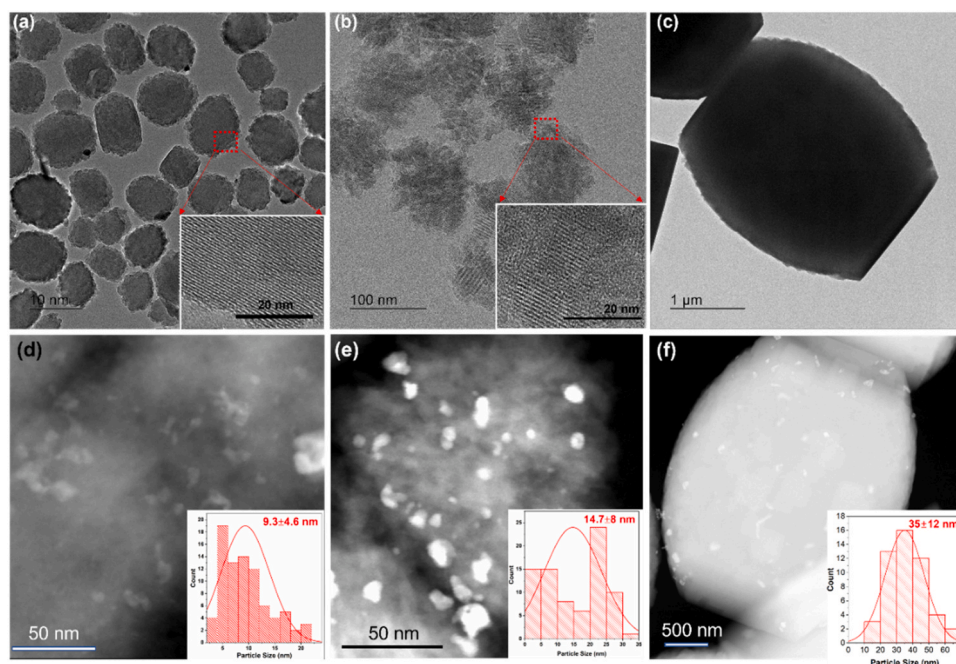

Fig. 2. HRTEM micrographs of (a) ZSM-5 NC, (b) ZSM-5 NS, (c) ZSM-5 Con; STEM and Ru particle size distribution (PSD) the reduced (d) 1%Ru(out)/NC, (e) 1%Ru (out)/NS and (f) 1%Ru (out)/Con catalysts.

size of ~9.3 nm were distributed on the external surface of ZSM-5 nanocrystals, whilst Ru NPs on the 1%Ru(out)/NS were measured to be ~14.7 nm. Comparatively, on the ZSM-5 Con support, large Ru NPs of ~35 nm were identified. The results from STEM suggest that the small crystal sizes of ZSM-5 NC and NS as the supports are beneficial to reduce the sizes of the supported Ru NPs.

Since the interaction between Ru and ZSM-5 supports and chemical state of Ru species are important factors to influence the catalytic behaviour, H_2-TPR and XPS were performed to understand the effect of zeolite morphology on the Ru reducibility and oxidation states. As shown in Fig. 3a, Ru catalysts with different supports exhibit two main peaks at 190–200 °C (peak I) and 230–290 °C (peak II), corresponding to the weakly and strongly bound RuO_x species with the support, respectively [24]. Specifically, the 1%Ru(out)/NS catalyst showed a low reduction temperature peak at 194 °C, indicating a weak interaction between RuO_x and ZSM-5 nanosheet. Comparatively, 1%Ru(out)/Con catalyst showed a main reduction peak at 202 °C and a small shoulder at 268 °C, which can be attributed to reduction of Ru species with a broad particle size distribution (PSD) (Fig. 2f) [25]. For 1%Ru(out)/NC catalyst, the main reduction peak at ~230 °C suggested a stronger interaction between Ru and ZSM-5 nanocrystal compared with the conventional support and nanosheet based catalysts. Therefore, the interaction between Ru species and ZSM-5 supports were in the following order: 1%Ru(out)/NC > 1%Ru(out)/Con > 1%Ru(out)/NS.

The XPS spectra of the catalysts showed Ru3d peaks associated with Ru^{4+} (RuO_2) and Ru^{6+} (RuO_3) (Fig. S4). For 1%Ru(out)/NS, the Ru $3d_{5/2}$ binding energy (B.E.) was observed at 281.2 eV corresponding to a Ru^{4+} (RuO_2) phase [6,26]. In the case of 1%Ru(out)/NC and 1%Ru(out)/Con, Ru $3d_{5/2}$ features at 280.4–280.8 eV for Ru^{4+} and at 281.7–282.4 eV for Ru^{6+} were observed which may be associated with the stronger interactions between Ru and zeolite compared with the NS based catalyst. Table S1 summarises the values of $Ru^{6+}/(Ru^{4+}+Ru^{6+})$ determined by analysis of the XP spectra of each of the catalysts which indicates the strength of the interaction between Ru and the support. The ratios were in the order: 1%Ru(out)/NC (49.2%) > 1%Ru(out)/Con (43.5%) > 1%Ru(out)/NS (0%) which is in line with the results from H_2-TPR. However, based on the catalytic performance above (Fig. 1, e. g., 1%Ru(out)/NS was more active than 1%Ru(out)/Con), the findings here indicate that the interactions between Ru and ZSM-5 supports might not play a key role in the NTP-catalysis. The 1Ru(out)/NC catalyst was selected (due to its good activity in the NTP catalysis) to investigate the stability of the catalyst by checking the changes in the chemical state of the Ru species before and post the plasma-catalytic CO_2 hydrogenation. Fig. S5 compares the XPS spectra of the calcined, reduced and spent 1Ru(out)/NC catalysts. Compared to the calcined 1Ru(out)/NC catalyst regarding the Ru^{4+} and Ru^{6+} species (Figs. S4 and S5), the reduced 1Ru(out)/NC catalyst showed a Ru $3d_{5/2}$ binding energy at 279.8 eV, corresponding to the Ru^0 phase, suggesting the complete reduction of Ru species by the H_2 plasma. Similarly, the XPS spectrum of the spent 1Ru(out)/NC catalyst shows the presence of Ru^0 species only, demonstrating
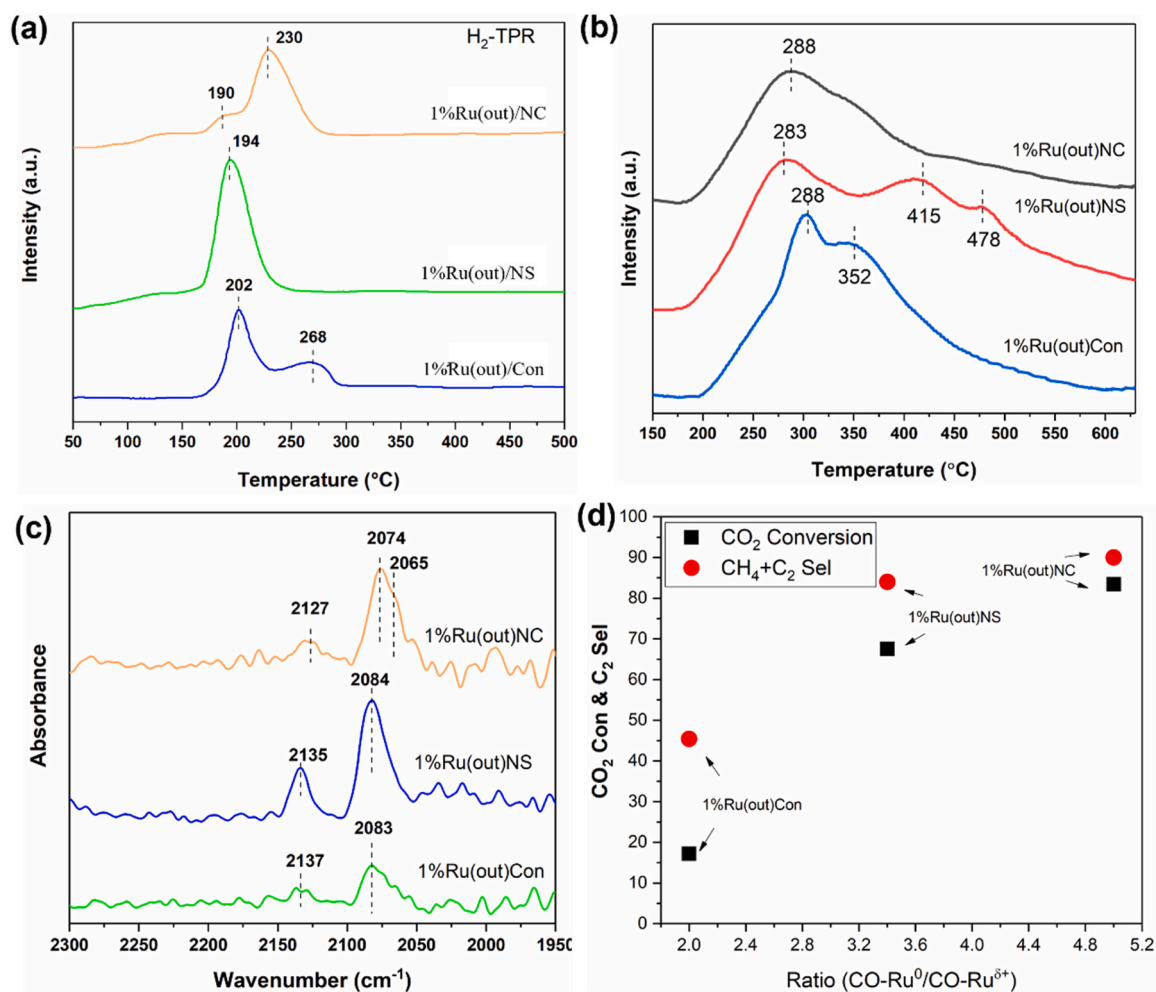
Fig. 3. (a) H_2-TPR profiles and (b) CO_2-TPD profiles for the 1%Ru(out)/NC, 1%Ru(out)/NS and 1%Ru(out)/Con catalysts, (c) CO-DRIFT spectra of the reduced 1%Ru(out)/NC, 1%Ru(out)/NS and 1%Ru(out)/Con catalysts at room temperature, and (d) the correlations between the catalyst activity at SIE of 32 J mL^{-1} and the CO adsorbed configuration from CO DRIFTS.

that Ru NPs are very stable during the NTP catalysis.

The interaction of CO_2 with the catalysts was investigated by CO_2-TPD, and the results are shown in Fig. 3b. A CO_2 desorption peak at 283–350 °C was observed from all the catalysts, corresponding to the desorption of moderately bound CO_2, whilst the high-temperature peak at 415–478 °C for 1%Ru(out)/NS could be attributed to the desorption of the strongly adsorbed CO_2 molecule [16,27]. The total amount of CO_2 adsorption was calculated to be 112.7, 135 and 175.1 μmol g^{-1} for 1Ru (out)/NC, 1Ru(out)/Con and 1Ru(out)/NS, respectively (Table S2). These findings cannot be correlated well with the catalytic activity where 1%Ru(out)/NC > 1%Ru(out)/NS > 1%Ru(out)/Con under the NTP condition. This result indicates that the effect of CO_2 adsorption properties on plasma-catalytic CO_2 hydrogenation is unlikely to be rate determining.

DRIFT spectroscopy with CO over reduced catalysts was used to probe the oxidation state and form of the Ru sites (Fig. 3c). The bands observed at 2065–2085 cm^{-1} are attributed to linearly adsorbed CO on the Ru^0, while the IR bands located at 2125–2140 cm^{-1} can be assigned to the tri-carbonyl species on partially oxidized Ru sites ($Ru^{\delta+}(CO)_3$ type) [6,28,29] which represent stronger and weaker binding of the CO to the surface, respectively [30],[31]. Table S3 summarises the ratio of peak areas of $Ru^0(CO)/Ru^{\delta+}(CO)_3$ which can be correlated with the strength of interaction of CO in the order 1%Ru(out)/NC (5.0) > 1%Ru (out)/NS (3.4) > 1%Ru(out)/Con (2.0) catalysts. Plotting these results against the CO_2 conversion and product selectivity of light hydrocarbons (CH_4 and C_2H_6, Fig. 3d), suggests that strong interaction with CO on the catalyst surface leads to an increased formation of CH_4 and light hydrocarbons. This is consistent with previous studies, which showed that CO is an active intermediate for methane formation [6,7,32], and the simultaneous plasma induced CH_x species from the formed CH_4 will interact via gas-phase carbon-chain-growth reactions to produce C_2 hydrocarbons [33]. In addition, the presence of small Ru NP sizes and their strong interaction with CO may explain the relative high performance of the catalysts in the NTP-catalytic CO_2 hydrogenation regarding

the formation of methane and C_2H_6 hydrocarbons.

3.2. Effect of Ru location and particle size

The findings above suggest that small Ru NPs are beneficial to NTP-catalytic CO_2 hydrogenation to methane and C_2 products. Compared to the metal NPs supported on the external surface of a zeolite carrier, confinement of metallic NPs using zeolite frameworks could reduce NP sizes and prevent metal aggregation during synthesis and catalysis [34]. Such confined and highly dispersed metal NPs within porous zeolites are beneficial to thermal catalysis [35]. Comparatively in NTP catalysis, the lifetime of the plasma-induced activated species is short, and it is likely that they lose energy due to collisional quenching during transport to the active site reducing significantly their activity [36]. Therefore, the trade-off between the accessibility (of the metallic NPs) and the size of NPs in porous catalysts is one of the key methods to optimise the performance of NTP-catalysis.

To investigate this aspect, ZSM-5 conventional support was used to prepare the Ru catalysts with Ru NPs on different locations, that is, encapsulated Ru NPs within its framework (0.5%Ru(in) and 1%Ru(in)), Ru NPs supported on its external surface (0.5% Ru(out)) and combination of the two (0.5%Ru(in)0.5%Ru(out)). TEM and elemental mapping analyses in Figs. 4 and S6 reveal the corresponding Ru NPs locations and PSDs in these catalysts. In detail, the Ru NPs of 0.5% Ru(out) were mainly dispersed on the external surface of ZSM-5 Con with a wide distribution and a large mean particle size of ~34 nm (Figs. 4a and S6a). Comparatively, the Ru NPs in 0.5%Ru(in) are primarily confined within ZSM-5 Con crystals with a narrow PSD cantered at ~6.3 nm (Figs. 4b and S6b). By doubling the Ru loading, small Ru NPs (average diameter of ~6.0 nm) were found sit close to the external surface of zeolite Con, indicating the improved accessibility of the Ru NPs in the resulting 1% Ru(in) catalyst than that in 0.5%Ru(in) (Figs. 4c and S6c). In the 0.5%Ru (in)0.5%Ru(out) catalyst, the Ru NPs located on the external surface are large with the diameters of ~34.4 nm (similar to the sizes found for the
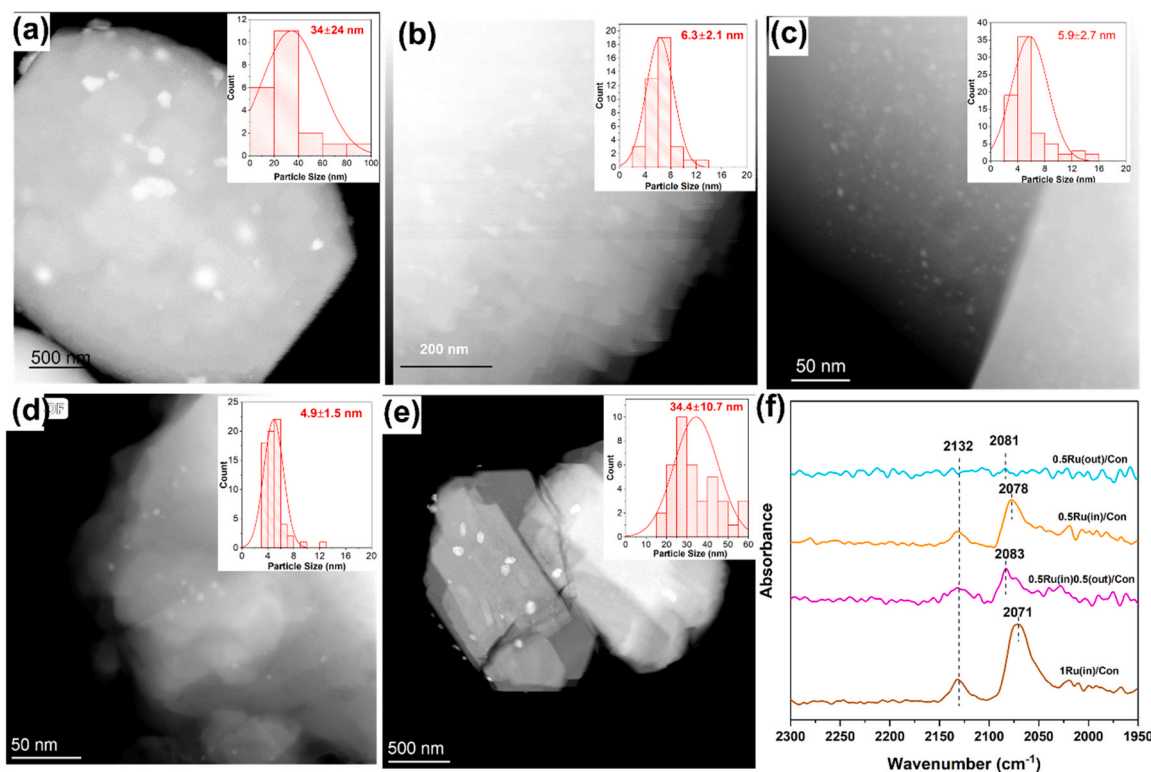
Fig. 4. STEM micrographs and particle size distribution (PSD) of (a) 0.5%Ru(out)/Con, (b) 0.5%Ru(in)/Con, (c) 1%Ru(in)/Con catalyst and (d-e) 0.5%Ru(out)0.5% Ru(in)/Con; (f) CO-DRIFT spectra of related reduced catalysts at room temperature.

0.5%Ru(out) catalyst), whilst the encapsulated Ru NPs had smaller diameters of ~5.0 nm (Fig. 4d and e).

XRD patterns of the 0.5%Ru(out)/Con, 0.5%Ru(in)/Con, 0.5%Ru(out)0.5%Ru(in)/Con and 1%Ru(in)/Con catalyst catalysts (Fig. S7) show the crystalline MFI structures and absence of characteristic diffraction peaks of Ru NPs (due to the low Ru loadings and/or highly dispersed Ru inside zeolite). N_2 physisorption analyses showed that all the catalysts had comparable porous properties (Fig. S8 and Table S3). Additionally, XPS analysis (Fig. S9 and Table S4) showed that encapsulated Ru catalysts (i.e., 0.5%Ru(in)/Con and 1%Ru(in)/Con catalysts) has more Ru^{6+} species with the ratio of $Ru^{6+}/(Ru^{4+}+Ru^{6+})$ of 42% and 45.6%, respectively, whereas the value of the ratio over 0.5%Ru(out)/Con and 0.5%Ru(out)0.5%Ru(in)/Con are 31.4% and 28.6%, respectively, suggesting the stronger interactions between Ru species with zeolite in the encapsulated catalysts. The CO DRIFTS spectrum in Fig. 4f shows no characteristic peaks of CO adsorption over 0.5% Ru(out)/Con, indicating a weak interaction between Ru and CO molecule, whilst 0.5% Ru(in)0.5%Ru(out) and 0.5% Ru(in) have a linear adsorbed CO peak at 2078–2083 cm^{-1}, originating from the stronger interaction between some small Ru NPs (likely the encapsulated and externally distributed ones, Fig. S6b and c) with CO molecule. The ratio of the peak areas for $Ru^0(CO)/Ru^{\delta+}(CO)_3$ over the 0.5%Ru(in), 0.5%Ru(in)0.5%Ru(out) and 1%Ru(in) catalysts were found to be ~3.9, 3.0 and 4.8, respectively (Table S5), indicating that the small Ru species has a relative strong interaction with CO molecule.

The catalysts (Fig. 4) were assessed in NTP-catalytic CO_2 hydrogenation to probe the effect of Ru NPs location and particle size on the NTP-catalysis. As shown in Fig. 5a, CO_2 conversions over all the catalysts were improved with an increase in the input energy, as expected. For the 0.5%Ru(out) catalyst with the large Ru NPs on the external surface, the CO_2 conversion increased by 62.7%, i.e., from 13.7 to 22.3% on increasing the SIE from 16 to 32 J mL^{-1}, whereas CO_2 conversion over the 0.5%Ru(in) catalyst increased by 357%, i.e., from 10.5 to 47.9%. However, it is interesting that at a low SIE of 16 J mL^{-1} (Fig. 4a), the 0.5%Ru(out) catalyst showed higher CO_2 conversions compared with the 0.5%Ru(in) catalyst (e.g., 13.7% vs. 10.5%), despite the significant difference in Ru NP sizes. Over the 0.5%Ru(in)0.5%Ru(out) catalysts, a comparable CO_2 conversion of ~13.2% (to ~13.7% achieved by 0.5%Ru (out)) was found at 16 J mL^{-1}, suggesting that encapsulated Ru active sites did not contribute to CO_2 conversion significantly at the low SIEs. However, by increasing the SIE to 32 J mL^{-1}, CO_2 conversion of the 0.5%Ru(in) and 0.5%Ru(in)0.5%Ru(out) system increased to ~47.9% (i.e., by 357%) and ~54% (i.e., by 309%), respectively, whilst that of the 0.5%Ru(out) system only increased to ~22% (i.e., by 62.7%), confirming that the encapsulated small Ru active sites contributed significantly to the increased CO_2 conversions at a high SIE. The findings above suggest that, at low SIEs, gas ionization is low, leading to the limited availability of the NTP-induced active species (e.g., vibrational activated CO_2 and CO*) in the gas discharge. Consequently, they prefer to interact with the exposed Ru NPs on the external surface with less diffusion resistance (compared to the encapsulated Ru NPs within the zeolite framework), that is, the external exposed Ru species dominate the CO_2 conversion at low SIEs in the present system [15]. Conversely, at a higher input energy (with sufficient short-lived reactive species
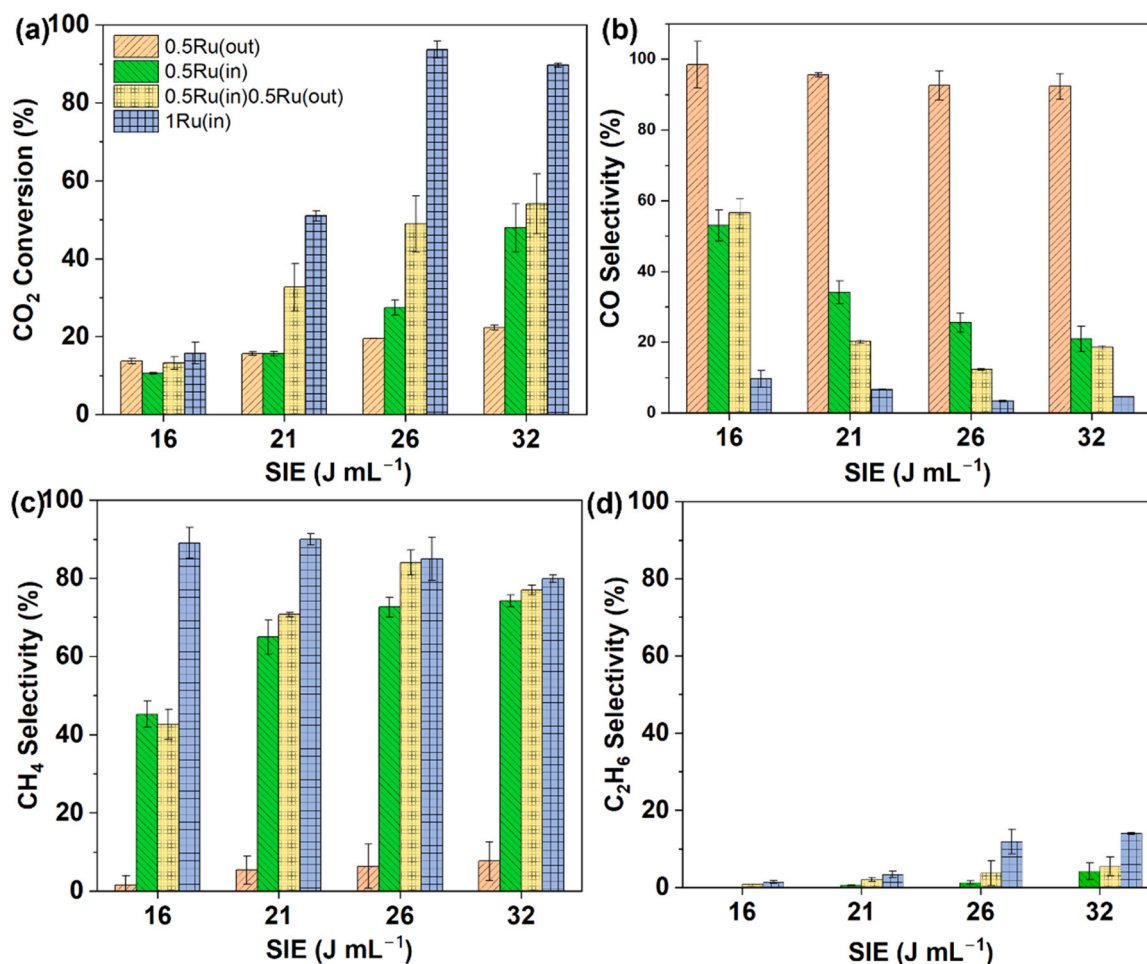

Fig. 5. Performance of NTP-activated CO_2 hydrogenation as a function of SIE over the 0.5%Ru(out)/Con, 0.5%Ru(in)/Con, 0.5%Ru(out)0.5%Ru(in)/Con and 1%Ru (in)/Con catalyst: (a) CO_2 conversion, (b) CO selectivity, (c) CH_4 selectivity and (d) C_2H_6 selectivity.

produced by NTP), the diffusion of these species to the internal of the porous catalysts to interact with the encapsulated Ru NPs is enhanced, making the encapsulated Ru NPs dominating sites to direct the CO_2 conversion.

Regarding the product selectivity, the system employing 0.5%Ru (out) (i.e., the catalyst with the weakest interaction with CO) showed high selectivity to CO (>90%) at different SIEs (Fig. 5b) with the low selectivity to CH_4 (i.e., ≤7.7%, Fig. 5c). The high selectivity of CO is due to the weak interactions between Ru species with CO molecule (as shown in Fig. 4f), which lead to the formed CO on the catalyst surface desorbing back to the gas phase as the product and inhibiting further hydrogenation of CO to form methane. In comparison with the other catalytic systems under investigation, C_2 hydrocarbons were not formed over the 0.5%Ru(out) system (since CH_4 formation was limited). The findings suggest that the low activity of the 0.5%Ru(out) catalyst may be explained by its weak interaction with CO (Fig. 4f). In detail, the large Ru NPs (~34 nm) on 0.5%Ru(out)/Con have low Ru surface area, and their ability to interact with CO molecule (from CO_2 dissociation in gas discharge) for surface hydrogenation reactions is rather poor (though they are highly accessible), and thus making CO as the main product. In comparison, with an increase in the SIE, the 0.5%Ru(in) catalyst suppressed the selectivity to CO (i.e., from 53% at 16 J mL^{-1} to 20.9% at 32 J mL^{-1}), and improved the selectivity to CH_4 and C_2H_6, as shown in Fig. 5c and d. The same phenomena were found for the system employing 0.5%Ru(in)0.5%Ru(out) as well, e.g., CH_4 selectivity increased from 42.6% at 16 J mL^{-1} to 77.5% at 32 J mL^{-1}.

Based on the findings and discussion above, for plasma activated CO_2 hydrogenation, the input plasma energy and the location of Ru NPs (corresponding to accessibility of active sites to energetic species) are major factors determining the CO_2 conversion. However, regarding the product selectivity of the NTP-catalysis, this is thought to be primarily controlled by the nature of metallic sites (i.e., as shown above, the system employing large Ru NPs promoted CO formation, whilst that employing the small Ru NPs were selective to CH_4 since the latter could stabilize the energetic intermediates, especially CO*, for selective surface reactions). This is further evidenced by the 1%Ru(in) catalyst with small Ru particles exposed on the external surface (according to STEM) and the increased Ru loading. In detail, at 16 J mL^{-1}, 1%Ru(in) showed a similar CO_2 conversion of 15.7% in comparison with 0.5%Ru(out) 0.5%Ru(in), however, it increased to ~89.7% (i.e., by 471%) at 32 J mL^{-1}. Compared to the 0.5%Ru(in)0.5%Ru(out) catalyst with large Ru particles on the external surface, the external small Ru NPs 1%Ru(in) catalyst is beneficial to interact with the reactive species (e.g., CO*) to produce CH_4 and thus contributing to the high CH_4 selectivity (>80%), as well as the selectivity to C_2H_6 (about 14%, at 32 J mL^{-1}). Therefore, the activity of the catalysts under investigation at high input energy, i.e., CO_2 conversions and CH_4 and C_2 selectivity, was mainly affected by the size of the Ru NPs with the following order: 1%Ru(in)> 0.5%Ru(in) 0.5%Ru(out)> 0.5%Ru(in)> 0.5%Ru(out). The above findings suggested that although the activity of the NTP-induced energetic species could be affected by molecular diffusion (especially at low input energy), the intrinsic characteristic of the catalyst is important as well to promote the conversion of substrates under the NTP conditions (especially at the high NTP input energy).

For the purpose of comparison, the developed catalysts were assessed for CO_2 hydrogenation under thermal conditions, as shown in Fig. S10. In addition, Joule heating during the NTP catalysis might also affect the chemical conversion, hence, the average bulk temperatures of the NTP systems at SIE of 16–32 J mL^{-1} were measured by an IR thermometer, which were ~65, ~105, ~120 and ~135 °C, respectively. As shown in Fig. S10, such low bulk temperatures of the NTP systems (i.e., <150 °C) could not activate CO_2 hydrogenation thermally. As shown in Fig. S10, for all the catalysts here an increase in the reaction temperature led to the increase in CO_2 conversions (Fig. S10a). At 450 °C, the 1%Ru(in) and 0.5%Ru(in) catalysts showed better CO_2 conversions of ~72% and ~69%, respectively, than 0.5%Ru(in)0.5%Ru(out) and 0.5%Ru(out) of

57% and 42.1%, suggesting that 1%Ru(in) and 0.5%Ru(in) have better intrinsic activity than the other two. Being different from the NTP-catalysis, in the thermal catalytic CO_2 hydrogenation, all the catalysts are selective to CH_4 (with the selectivity >65%) over the temperature range from 250 to 450 °C (Fig. S10b). With an increase in reaction temperature, the selectivity to CO over all the catalysts increased, especially 0.5%Ru(out), on which the CO selectivity increased to ~34% at 450 °C (Fig. S9c), consistent with the calculated increase trend of CO formation at high temperature (Fig. S10d). Regarding the variation in the CO selectivity over 0.5%Ru(out), it could be ascribed to fast desorption of weakly interacted CO from the catalyst surface, whilst the 1%Ru(in), 0.5%Ru(in)0.5%Ru(out) and 0.5%Ru(in) catalysts showed comparable CO selectivity of < 10%. The order of activity of the catalysts in CO_2 hydrogenation under thermal conditions correlates well with the Ru dispersion, in which the highly dispersed Ru NPs encapsulated in ZSM-5 zeolite contributed to the good performance of selective CO_2 conversion. Therefore, the findings above show that the catalyst with the high Ru dispersion is beneficial to the catalysis under both thermal and NTP conditions and suggest that the development of relevant catalysts with highly dispersed metal active sites (e.g., sub-nanosized clusters, even single-atoms/sites) situated on/near the external surface may be suitable for enhancing the NTP-catalysis. It is also worth noting that, in contrast with the observations using NTP activation, thermal activation does not result in the formation of C2 hydrocarbons. This indicates that the Ru NPs in the four catalysts are intrinsically selective to CH_4, and the formation of C_2H_6 in the NTP systems could be attributed to the CH_4 coupling reactions in plasma gas discharge (to be further discussed later).

3.3. Mechanism of NTP-catalytic CO_2 hydrogenation over Ru catalysts

Catalytic CO_2 hydrogenation to methane can be achieved via three possible mechanisms:

  (i) CO_2 was converted to carbonyl (CO) species with subsequent formation of oxygenate species such as the carbonates and formates (*HCOO) intermediate;
  (ii) direct dissociation of CO_2 to CO* and atomic oxygen on the catalyst surface, followed by CO* hydrogenation;
  (iii) dissociation of CO_2, followed by further dissociation of CO* to C* and hydrogenation of surface bounded C* [37–39].

Herein, comparative in situ DRIFTS characterisation of the four catalysts was performed to understand the reaction pathways of catalytic CO_2 hydrogenation under the NTP condition.

Under the plasma-off condition with feed gas at room temperature, surface carbonate species with the characteristic IR bands at 1624–1697 and 1340–1352 cm^{-1} were observed over all the catalysts, as shown in Fig. S11, due to the CO_2 interaction with the surface hydroxyl group on the catalyst [6]. Upon the plasma ignition (Fig. 6a–d), the peaks at 1850–1865, 1940–1945, 2040–2070 and 2196 cm^{-1} were observed, which are characteristic wavenumbers of the adsorbed CO with bridge, linear and multi-bonded configurations on the Ru NPs [40]. This suggests that CO species may be key intermediates for the catalytic conversion of CO_2 [7]. Specifically, on the 1%Ru(out)/NC catalyst, characteristic bands at 1750 cm^{-1} (corresponding to the adsorbed *HCO species [39]), and the bands at 1591, 1312 and 1197 cm^{-1} (corresponding to the v_{as} (OCO), v_s (OCO) and v_s (C-O) from bidentate formate species (*HCOO) species [40,41]), increased with time, indicating that plasma-induced H* species could react with the carbonate species to produce the carbon-related active intermediates towards methane. The presence of the bands at 2964 and 1000 cm^{-1} from *CH_3 and C-O stretching from methoxy species (*H_3CO) suggested the formation of methane [39]. However, the *CH_3 species were not observed over other three catalysts since methane can be desorbed quickly from catalyst surface under NTP conditions [6,42], suggesting that the 1%Ru(out)/NC
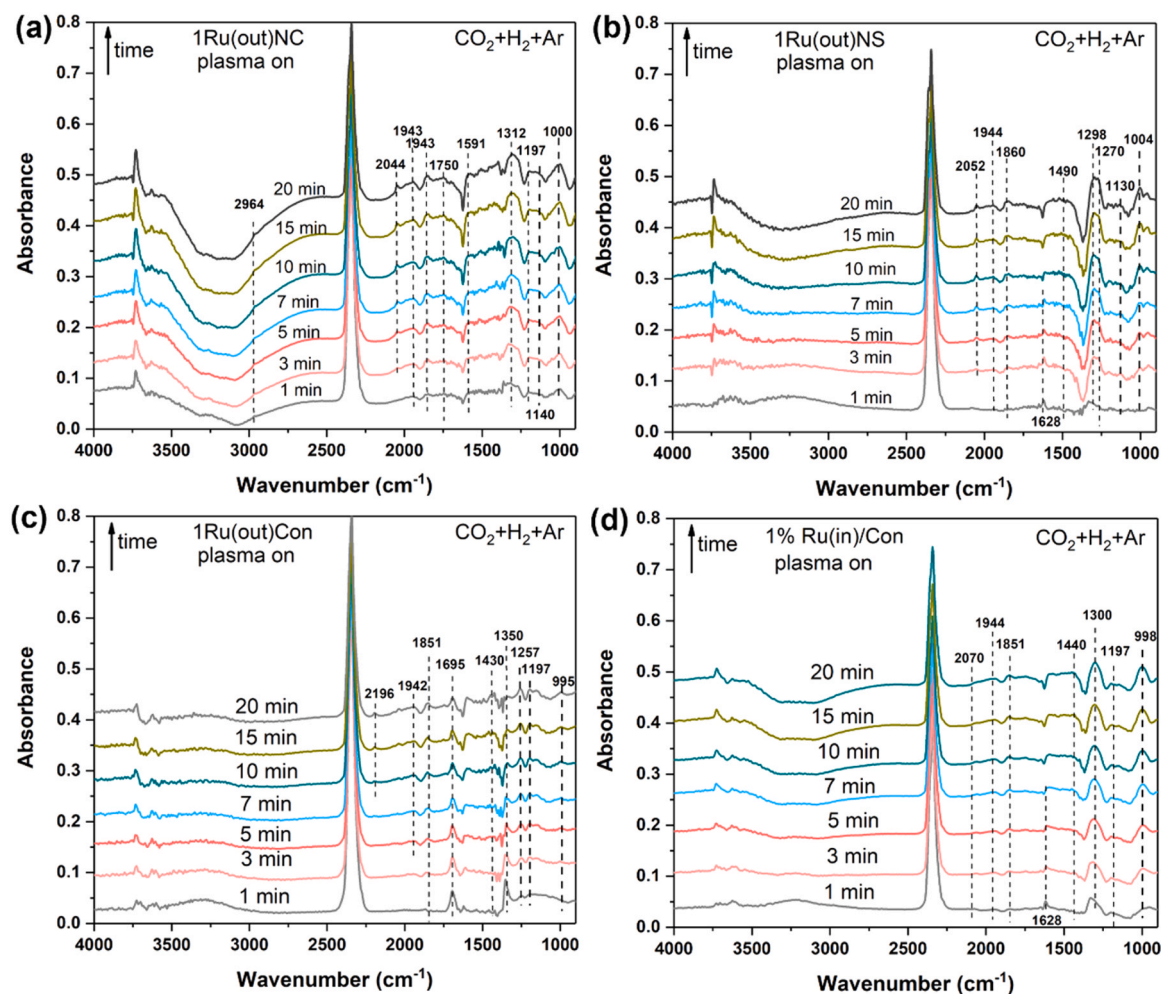
Fig. 6. *In situ* DRIFTS spectra of surface species under plasma-on condition with the feed gas of 3% CO_2 + 12% H_2 + Ar (4.5 kV, 28 kHz) on (a) 1%Ru(out)/NC, (b) 1%Ru(out)/NS, (c) 1%Ru(out)/Con and (d) 1%Ru(in)/Con.

catalyst had the strongest interaction with the intermediate to produce methane. Thus, under the NTP conditions, CO_2 hydrogenation to CH_4 over the 1%Ru(out)/NC catalyst could produce CO, formyl and formate species as intermediates towards methane formation. Comparatively, in the system employing 1%Ru(out)/NS and 1%Ru(in)/Con, the characteristics of the DRIFTS data are similar. In detail, the bands of bicarbonate species at 1628 cm^{-1} ($v_{as}(CO_3)$) was found to disappear gradually, whilst another three bands located at 1440–1560 cm^{-1} (v_{as} (OCO)), 1270–1300 cm^{-1} (v_s (OCO)), and 1130–1197 cm^{-1} (v_s(C-O)), corresponding to formate species [41], increased continuously over time. Thus, under the NTP conditions, CO_2 hydrogenation to CH_4 over the 1%Ru(out)/NS and 1%Ru(in)/Con could produce CO and formate species as intermediates. Conversely, in the system over the 1%Ru (out)/Con catalyst, no linearly adsorbed CO* species (at 2040–2070 cm^{-1}) was observed, agreeing with the results by CO-DRIFTS (Fig. 3c). Also, the intensity of carbonate at 1695 cm^{-1} did not change and that related to formate species was rather weak in comparison with that in other three systems, explaining its relatively poor activity for NTP-catalytic CO_2 hydrogenation (Fig. 5).

Regarding the formation of the C_2 product, based on the activity results from Figs. 1 and 5, a higher SIE reduced the selectivity to CO and CH_4 and increased the selectivity to C_2H_6. This suggests that CO and methane are primary products from plasma-catalytic CO_2 hydrogenation, whilst C_2 hydrocarbons are by-products from methane coupling reactions through the gas-phase reactions between plasma activated $CH_x^{\bullet}$ species (e.g., $CH_3^{\bullet}$ and $CH_2^{\bullet}$ species) [33]. This can be evidenced by the

DRIFTS results that no peak of surface CH_x species were observed, suggesting that the further activation of the desorbed CH_4 in the gas phase discharge formed $CH_x^{\bullet}$ species for CH_4 coupling to form the C_2 by-product, especially at high SIE with high CH_4 yield. Therefore, CO_2 hydrogenation is selectively converted to CH_4 over the Ru catalysts, and desorbed back to gas discharge to $CH_3^{\bullet}$ species, which were subsequently converted to C_2H_6 in gas phase, in line with previous findings [21,33].

4. Conclusions

Catalyst design is a crucial aspect for improving relevant plasma-catalysis systems to advance the hybrid technology. Findings of the study demonstrated the significant effect of the morphology of ZSM-5 supports and the location of Ru NPs on NTP-catalytic CO_2 hydrogenation, especially the product selectivity. Compared to the conventional large ZSM-5 support (~621 nm), the ZSM-5 nanostructures (of nanocrystals and nanosheets, ~120 nm) were found to improve the dispersion of Ru NPs after the impregnation synthesis, being able to interact with CO molecule strongly, and thus promoting the surface reactions towards methane formation. For example, at the specific energy input of at 32 J mL^{-1}, the 1%Ru(out)/NC catalyst promoted the CO_2 conversion and CH_4 selectivity of 83.4% and 74%, whilst that over 1%Ru(out)/Con was 17.2% and 45.5%, respectively. Based on the conventional ZSM-5, impregnation and/or encapsulation syntheses were employed to prepare the catalysts with Ru NPs on different locations (including the encapsulated Ru NPs within the framework, Ru NPs supported on the

external surface and combination of the two) to probe the effect of the location of Ru NPs on the NTP-catalysis. The results show that the encapsulated 1%Ru(in) catalyst with small Ru NPs distributed across on the internal and external space of the zeolite support demonstrated the best performance at high plasma input energy, with the high activity for CO_2 conversion of 89.7% and high selectivity to CH_4 of 80% and C2 product of 14% at 32 J mL^{-1}.

The findings of the study suggest that (i) the intrinsic property of the metal catalysts such as particle sizes and interactions with CO is crucial to control the product selectivity for NTP-catalytic CO_2 hydrogenation, (ii) the location of metal active sites in the porous catalyst determines its accessibility to the plasma-induced reactive species, especially at low input plasma energy, and (iii) a catalyst with small metal Ru NPs highly dispersed on the outer surface might be beneficial to NTP-catalysis. This work demonstrates the effect of catalyst design on the NTP-activated CO_2 hydrogenation and paves the way to the further development of bespoke porous materials supported metal catalysts for improving NTP-catalytic systems.

CRediT authorship contribution statement

Chansai Sarayute: Investigation, Methodology, Supervision, Writing – review & editing. **Hardacre Christopher:** Formal analysis, Funding acquisition, Methodology, Resources, Supervision, Writing – review & editing. **Wattanakit Chularat:** Funding acquisition, Supervision, Writing – review & editing. **Fan Xiaolei:** Conceptualization, Formal analysis, Funding acquisition, Methodology, Project administration, Resources, Supervision, Writing – review & editing. **Xu Shanshan:** Conceptualization, Formal analysis, Investigation, Methodology, Writing – original draft, Visualization. **Dugkhuntod Pannida:** Formal analysis, Investigation, Writing – original draft. **Ding Shengzhe:** Investigation, Writing – review & editing. **Zhang Yuxin:** Investigation, Writing – review & editing. **Gosalvitr Piya:** Supervision, Writing – review & editing. **Chen Shaowei:** Formal analysis, Investigation, Writing – original draft. **Huang Jianguo:** Supervision, Writing – review & editing. **Klinyod Sorasak:** Supervision, Writing – review & editing.

Declaration of Competing Interest

Herein we confirm that all authors whom contributed to this work have no conflict of interest.

Data availability

Data will be made available on request.

Acknowledgements

Appendix A. Supporting information

Supplementary data associated with this article can be found in the online version at doi:10.1016/j.apcatb.2024.123826.

References

[1] S. Roy, A. Cherevotan, S.C. Peter, Thermochemical CO_2 hydrogenation to single carbon products: scientific and technological challenges, ACS Energy Lett. 3 (2018) 1938–1966.
[2] A. Bogaerts, X. Tu, J.C. Whitehead, G. Centi, L. Lefferts, O. Guaitella, F. Azzolina-Jury, H.-H. Kim, A.B. Murphy, W.F. Schneider, T. Nozaki, J.C. Hicks, A. Rousseau, F. Thevenet, A. Khacef, M. Carreon, The 2020 plasma catalysis roadmap, J. Phys. D Appl. Phys. 53 (2020) 443001.
[3] E.C. Neyts, K.K. Ostrikov, M.K. Sunkara, A. Bogaerts, Plasma catalysis: synergistic effects at the nanoscale, Chem. Rev. 115 (2015) 13408–13446.
[4] J.C. Whitehead, Plasma-catalysis: is it just a question of scale? Front. Chem. Sci. Eng. 13 (2019) 264–273.
[5] M. Nizio, R. Benrabbah, M. Krzak, R. Debek, M. Motak, S. Cavadias, M.E. Gálvez, P. Da Costa, Low temperature hybrid plasma-catalytic methanation over Ni-Ce-Zr hydrotalcite-derived catalysts, Catal. Commun. 83 (2016) 14–17.
[6] S. Xu, S. Chansai, Y. Shao, S. Xu, Y.-C. Wang, S. Haigh, Y. Mu, Y. Jiao, C.E. Stere, H. Chen, Mechanistic study of non-thermal plasma assisted CO_2 hydrogenation over Ru supported on MgAl layered double hydroxide, Appl. Catal. B Environ. 268 (2020) 118752.
[7] Y. Gao, L. Dou, S. Zhang, L. Zong, J. Pan, X. Hu, H. Sun, K. Ostrikov, T. Shao, Coupling bimetallic Ni-Fe catalysts and nanosecond pulsed plasma for synergistic low-temperature CO_2 methanation, Chem. Eng. J. 420 (2021) 127693.
[8] Y. Wang, W. Yang, S. Xu, S. Zhao, G. Chen, A. Weidenkaff, C. Hardacre, X. Fan, J. Huang, X. Tu, Shielding protection by mesoporous catalysts for improving plasma-catalytic ambient ammonia synthesis, J. Am. Chem. Soc. 144 (2022) 12020–12031.
[9] Y. Zhang, S. Li, Z. Yuan, H. Chen, X. Fan, Mechanochemical synthesis of RuCo/MgTiO3 catalysts for nonthermal plasma-assisted ammonia synthesis, Ind. Eng. Chem. Res. 61 (2022) 14199–14210.
[10] C.E. Stere, J.A. Anderson, S. Chansai, J.J. Delgado, A. Goguet, W.G. Graham, C. Hardacre, S.R. Taylor, X. Tu, Z. Wang, Non-thermal plasma activation of gold-based catalysts for low-temperature water–gas shift catalysis, Angew. Chem. Int. Ed. 56 (2017) 5579–5583.
[11] S. Xu, S. Chansai, C. Stere, B. Inceesungvorn, A. Goguet, K. Wangkawong, S. R. Taylor, N. Al-Janabi, C. Hardacre, P.A. Martin, Sustaining metal–organic frameworks for water–gas shift catalysis by non-thermal plasma, Nat. Catal. 2 (2019) 142–148.
[12] Q. Sun, N. Wang, J. Yu, Advances in catalytic applications of zeolite-supported metal catalysts, Adv. Mater. 33 (2021) e2104442.
[13] Y. Zhang, H.-y Wang, Y.-r Zhang, A. Bogaerts, Formation of microdischarges inside a mesoporous catalyst in dielectric barrier discharge plasmas, Plasma Sources Sci. Technol. 26 (2017) 054002.
[14] Y.-R. Zhang, E.C. Neyts, A. Bogaerts, Enhancement of plasma generation in catalyst pores with different shapes, Plasma Sources Sci. Technol. 27 (2018) 055008.
[15] H. Chen, F. Goodarzi, Y. Mu, S. Chansai, J.J. Mielby, B. Mao, T. Sooknoi, C. Hardacre, S. Kegnæs, X. Fan, Effect of metal dispersion and support structure of Ni/silicalite-1 catalysts on non-thermal plasma (NTP) activated CO_2 hydrogenation, Appl. Catal. B Environ. 272 (2020) 119013.
[16] H. Chen, Y. Mu, Y. Shao, S. Chansai, S. Xu, C.E. Stere, H. Xiang, R. Zhang, Y. Jiao, C. Hardacre, X. Fan, Coupling non-thermal plasma with Ni catalysts supported on BETA zeolite for catalytic CO_2 methanation, Catal. Sci. Technol. 9 (2019) 4135–4145.
[17] M.C. Bacariza, M. Biset-Peiró, I. Graça, J. Guilera, J. Morante, J.M. Lopes, T. Andreu, C. Henriques, DBD plasma-assisted CO_2 methanation using zeolite-based catalysts: structure composition-reactivity approach and effect of Ce as promoter, J. CO_2 Util. 26 (2018) 202–211.
[18] Y.-R. Zhang, K. Van Laer, E.C. Neyts, A. Bogaerts, Can plasma be formed in catalyst pores? A modeling investigation, Appl. Catal. B Environ. 185 (2016) 56–67.
[19] H. Chen, H. Lee, S. Chen, Y. Chao, M. Chang, Review of plasma catalysis on hydrocarbon reforming for hydrogen production—interaction, integration, and prospects, Appl. Catal. B Environ. 85 (2008) 1–9.
[20] S. Xu, S. Chansai, S. Xu, C.E. Stere, Y. Jiao, S. Yang, C. Hardacre, X. Fan, CO poisoning of Ru catalysts in CO_2 hydrogenation under thermal and plasma conditions: a combined kinetic and diffuse reflectance infrared Fourier transform spectroscopy–mass spectrometry study, ACS Catal. 10 (2020) 12828–12840.
[21] L. Lan, A. Wang, Y. Wang, CO_2 hydrogenation to lower hydrocarbons over ZSM-5-supported catalysts in a dielectric-barrier discharge plasma reactor, Catal. Commun. 130 (2019) 105761.
[22] B. Ashford, C.-K. Poh, K. Ostrikov, L. Chen, X. Tu, Plasma-catalytic CO_2 hydrogenation to ethane in a dielectric barrier discharge reactor, J. CO_2 Util. 57 (2022) 101882.
[23] L. Meng, X. Zhu, E.J.M. Hensen, Stable Fe/ZSM-5 nanosheet zeolite catalysts for the oxidation of benzene to phenol, ACS Catal. 7 (2017) 2709–2719.
[24] Y. Guo, S. Mei, K. Yuan, D.-J. Wang, H.-C. Liu, C.-H. Yan, Y.-W. Zhang, Low-temperature CO_2 methanation over CeO2-supported Ru single atoms, nanoclusters, and nanoparticles competitively tuned by strong metal–support interactions and H-spillover effect, ACS Catal. 8 (2018) 6203–6215.
[25] C. Gennequin, C. Poupin, E. Abi-Aad, R. Mahfouz, S. Aouad, J. Estephane, CO_2 methanation over Ru and/or Ni based catalysts Osupported on KIT-6, Al2O3 and CeO2, 2020, in: Proceedings of the Eleventh International Renewable Energy Congress (IREC), 2020, 1–5.
[26] D. Li, R. Li, M. Lu, X. Lin, Y. Zhan, L. Jiang, Carbon dioxide reforming of methane over Ru catalysts supported on Mg-Al oxides: a highly dispersed and stable Ru/Mg (Al)O catalyst, Appl. Catal. B Environ. 200 (2017) 566–577.

[27] A. Quindimil, U. De-La-Torre, B. Pereda-Ayo, J.A. González-Marcos, J.R. González-Velasco, Ni catalysts with La as promoter supported over Y- and BETA- zeolites for CO$_2$ methanation, Appl. Catal. B Environ. 238 (2018) 393–403.

[28] L. Chen, Y. Zhu, H. Zheng, C. Zhang, Y. Li, Aqueous-phase hydrodeoxygenation of propanoic acid over the Ru/ZrO$_2$ and Ru–Mo/ZrO$_2$ catalysts, Appl. Catal. A Gen. 411-412 (2012) 95–104.

[29] J. Zhou, Z. Gao, G. Xiang, T. Zhai, Z. Liu, W. Zhao, X. Liang, L. Wang, Interfacial compatibility critically controls Ru/TiO$_2$ metal-support interaction modes in CO$_2$ hydrogenation, Nat. Commun. 13 (2022) 327.

[30] B.T. Loveless, C. Buda, M. Neurock, E. Iglesia, CO chemisorption and dissociation at high coverages during CO hydrogenation on Ru catalysts, J. Am. Chem. Soc. 135 (2013) 6107–6121.

[31] S.Y. Chin, C.T. Williams, M.D. Amiridis, FTIR studies of CO adsorption on Al$_2$O$_3$- and SiO$_2$-supported Ru catalysts, J. Phys. Chem. B 110 (2006) 871–882.

[32] A. Karelovic, P. Ruiz, CO$_2$ hydrogenation at low temperature over Rh/γ-Al$_2$O$_3$ catalysts: effect of the metal particle size on catalytic performances and reaction mechanism, Appl. Catal. B Environ. 113-114 (2012) 237–249.

[33] J. Wang, M.S. AlQahtani, X. Wang, S.D. Knecht, S.G. Bilén, C. Song, W. Chu, One-step plasma-enabled catalytic carbon dioxide hydrogenation to higher hydrocarbons: significance of catalyst-bed configuration, Green Chem. 23 (2021) 1642–1647.

[34] H. Wang, L. Wang, F.S. Xiao, Metal@zeolite hybrid materials for catalysis, ACS Cent. Sci. 6 (2020) 1685–1697.

[35] S.M. Wu, X.Y. Yang, C. Janiak, Confinement effects in zeolite-confined noble metals, Angew. Chem. Int. Ed. Engl. 58 (2019) 12340–12354.

[36] S. Xu, H. Chen, X. Fan, Rational design of catalysts for non-thermal plasma (NTP) catalysis: a reflective review, Catal. Today 419 (2023) 114144.

[37] M. Marwood, R. Doepper, A. Renken, In-situ surface and gas phase analysis for kinetic studies under transient conditions: the catalytic hydrogenation of CO$_2$, Appl. Catal. A Gen. 151 (1997) 223–246.

[38] A. Solis-Garcia, J.F. Louvier-Hernandez, A. Almendarez-Camarillo, J.C. Fierro-Gonzalez, Participation of surface bicarbonate, formate and methoxy species in the carbon dioxide methanation catalyzed by ZrO2-supported Ni, Appl. Catal. B Environ. 218 (2017) 611–620.

[39] S. Eckle, H.-G. Anfang, R.Jr Behm, Reaction intermediates and side products in the methanation of CO and CO$_2$ over supported Ru catalysts in H2-rich reformate gases, J. Phys. Chem. C 115 (2011) 1361–1367.

[40] F. Villagra-Soza, S. Godoy, A. Karelovic, R. Jiménez, Scrutinizing the mechanism of CO$_2$ hydrogenation over Ni, CO and bimetallic NiCo surfaces: isotopic measurements, operando-FTIR experiments and kinetics modelling, J. Catal. 414 (2022) 1–15.

[41] J. Kondo, H. Abe, Y. Sakata, K.-i Maruya, K. Domen, T. Onishi, , Infrared studies of adsorbed species of H 2, CO and CO 2 over ZrO 2, J. Chem. Soc., Faraday Trans. 1 Phys. Chem. Condens. Phases 84 (1988) 511–519.

[42] H.-H. Kim, Y. Teramoto, A. Ogata, H. Takagi, T. Nanba, Plasma catalysis for environmental treatment and energy applications, Plasma Chem. Plasma Process. 36 (2015) 45–72.